

MECHANICAL AND ELECTROSTATIC DISPERSION OF A POLYDISPERSE CLUSTER OF DROPS FOR SOOT CONTROL

J. Bellan and K. Harstad
Jet Propulsion Laboratory
California Institute of Technology
4800 Oak Grove Drive
Pasadena, CA. 91109

ABSTRACT

A model is presented for the behavior of a polydisperse cluster of spherical evaporating drops in a cylindrical, axisymmetric inviscid vortex. The formulation accounts for drop interactions and for complete dynamic and thermodynamic coupling between drops and gas. The drops may or may not be electrostatically charged. When the drops are charged, the resulting electrostatic force is included in the drops momentum equations. Calculations are made for drops having benzene properties. For charged drops, the calculations are stopped at the Rayleigh limit. The results show that electrostatic dispersion is superior to drop-induced dispersion in decreasing the mass fraction of the evaporated compound and the gas density. This is because the electrostatic force maintains a large drop velocity angle at the outer edge of the cluster thus dispersing the drops more effectively while maintaining a finite slip velocity between drops and gas and promoting engulfment of hot air, both of which enhance evaporation. The relationship between these findings and soot control is discussed.

Key words: clusters of drops, dense sprays, soot control, polydisperse sprays, drops in a vortex

INTRODUCTION

This study investigates the potential of electrostatic liquid drop charging for dispersing drops in a combustionspray so as to avoid the creation of the fuel-rich-vapor regions where soot nucleation occurs. Experimental evidence of such sooting behavior has been presented by Law [1]. The relationship between drop dispersion and soot formation has been investigated by Sangiovanni [2] who observed streams of burning drops and showed that the soot emission index decreases monotonically with the spacing between drops for a variety of fuels and oxygen mass fractions in the surrounding gas. Since in Sangiovanni's study [2] it is only the effect of drop spacing in a single direction that has been investigated, those results underestimate the benefit of drop dispersion in a real spray where a drop is surrounded by other drops in all directions.

Evidence that electrostatic dispersion has the potential of achieving soot control is given by Bellan and Harstad [3]. Their numerical results show that both the evaporated fuel interstitial mass fraction, Y_{Fi} , and the interstitial gas density, ρ_{gi} , are lower during evaporation of electrostatically charged drops of three representative high-energy fuels in a cluster embedded into a vortex. Formation of soot precursors through nucleation reactions is directly associated with the partial density of the fuel in the gas phase [4], and thus a reduction of $Y_{Fi}\rho_{gi}$ is indicative of reduced soot nucleation. Furthermore, the results of Bellan and Harstad [3] show that liquid fuels with smaller latent heat are more prone to soot precursor formation because the ratio of the evaporation to dispersion time is smaller. Bellan and Harstad [3] also show that even a small amount of electrostatic charge (25% of the maximum possible with the spray triode [5]) has considerable effect upon the value of $Y_{Fi}\rho_{gi}$, and that the largest changes are obtained by charging (i.e. from 0% to 25% of the maximum charge) rather than by increasing the initial charge (to 50% or 75% of the maximum charge).

Here we determine what level of mechanical dispersion could affect the drops to the same degree as electrostatic dispersion, and explore the possibility of combining electrostatic drop dispersion with fluid mechanical methods, such as creation of turbulent vertical structures, in order to further mitigate soot formation.

DROPS AND GAS DYNAMICS

The physical configuration of the cluster of drops embedded into an axisymmetric vortex is depicted in Fig. 1 for an initial binary drop size distribution. Each drop initial-size-class distribution is followed in its own system of coordinates

moving with the drops, r_j , where j denotes the initial-size-class, whereas the gas is followed in its own system of coordinates, r . The cluster volume is bounded by surfaces which are the statistical envelopes of the outermost (R_c) and innermost (R_{in}) drops. The gas Reynolds number is defined as $Re = u_g R_c / \mu_g$ where u_g is gas velocity, R_c is cluster radius, and μ_g is gas viscosity; typically $Re \sim O(10^4)$ so that the vortex is inviscid. The drop Reynolds number is defined as $Re_{dj} = u_{sj} R_j / \mu_g$ where $u_{sj} = \bar{u}'_{sj} - \bar{u}'_g$ is the local slip velocity between phases, \bar{u}'_{dj} is the drop velocity and r_j is the drop radius. Initially, $Re_{dj} \sim O(1) - O(10)$ so that a drag force resulting from shape-drag, friction and drop evaporation causes interaction between drops and gas. The radial force due to the electrostatic charge is also included in the total force on the drops [3].

The concept of 'sphere of influence' [6] around each drop is used to model heat and mass transfer within and around each drop; the radius of the sphere of influence, R_i is defined statistically. The conservation equations for drops and gas, the turbulence model for both drops and gas, the pressure and dynamic drop-gas interaction model, the boundary and initial conditions, and the modeling of the electrostatic force contribution have all been described in detail elsewhere [7, 3]. What is given below is a concise summary of that model.

The drops are followed in Lagrangian systems of coordinates, r_j , whereas the gas is modeled in an Eulerian manner. Thus, for each initial-size-class, a set of equations is solved including the drop trajectory equation, the momentum equation, and an equation for the chop number in each computational annulus representing the discretization. The gas conservation equations are those for mass, momentum, energy and species coupled to the equation of state. Coupling of drops and gas occurs through boundary conditions at the chop surface (conservation of mass, momentum, energy, species and the Langmuir-Knudsen evaporation law) as well as through the drag term which is function of the slip velocity and a drag coefficient that accounts for evaporative blowing effects. Gas turbulence is modeled following the traditional Prandtl 'mixing length' approach with the laminar viscosity being enhanced by a turbulent contribution which is proportional to a constant C_T . Since order of magnitude estimates show that there are many Kolmogorov-type eddies between adjacent drops, drop turbulent diffusion is modeled in analogy with particle Brownian motion induced by thermal fluctuations [8]; the basic assumption is made that the characteristic velocity scales with cluster size and the fluctuations are here those of the small scale turbulent eddies. The pressure is modeled as a sum of several terms: an ambient, constant pressure, a pressure contribution from centrifugal effects potentially important at small distances from the vortex center, large length scale drop-gas interaction, and a pressure change due to convection. In this manner, the resulting radial component of the gas force correctly accounts for effects of cluster 'porosity' portraying the fact that the cluster appears to the surrounding gas as a porous material for which the drops represent the condensed phase. A velocity \bar{u}'_{cr} is associated with the average motion of the drops in the cluster such that in each annulus $\bar{u}'_{cr} = d\bar{r}'_c/dt$.

Boundary conditions

Since the cluster does not have a solid boundary with the surrounding gas, there is limited shear at the cluster boundary and no exceptionally large velocity gradients are expected near the boundaries. However, relatively large gradients in the mass fractions and gas temperature may exist. Heat and species in the cluster surroundings are assumed to diffuse and convect towards the cluster from a prescribed value at infinity. In all calculations there is no vapor of the evaporating compound in the far field and $T_{g\infty}(t) = T_{g\infty}^0 [1 + t/(6 \times 10^{-3})]$ in order to simulate the passage of the vortex through an increasing temperature region; $T_{gi}^0 = T_{\infty}$. Similarly, $Y_{Fi}^0 = Y_{F\infty}^0$.

If $u_{cr} > u_{gr}$, the cluster engulfs gas at a rate proportional to $[r_c \rho_g (u_{cr} - u_{gr})]_{r=R_c}$; if $u_{gr} > u_{cr}$ the cluster emits gas and only weak diffusion couples it to the surrounding gas. Equivalent arguments are valid for heat transfer. To model this situation, a Nusselt number approach is used where the correlation is $Nu_c = 1 + C_1 Pr_g Re_c$ and $Re_c = [\rho_g r_c \max(0, u_{cr} - u_{gr}) / (\mu_g + \mu_T)]_{r=R_c}$ is the effective Reynolds number. The power 1 is chosen for Pr_g and Re_c so that the expression for Nu_c agrees for $C_1 = 1$ with the engulfing/emitting process described above. Constant C_1 is a free, phenomenological parameter. Consistent with the similarity assumption $Sc_g = Pr_g$, the boundary condition for the evaporating species is

$$(r \partial Y_F / \partial r)_{r=R_c} = Nu_c (Y_{F\infty} - Y_{F,r=R_c}) \quad (9)$$

At the inner cluster boundary, $\partial Y_F / \partial r = \partial T_{gi} / \partial r = 0$. At the vortex center (taken to be an infinitesimally small radial distance to avoid singularities), the gradients of velocities and all dependent variables gradients vanish.

Initial conditions

The spatial dependence of n_j^0 and the global initial air/liquid mass ratio, Φ^0 , are prescribed to yield an initial chwp count [7]. Additional initial dependent variables to be prescribed are the drop temperature, T_{ds} , gas pressure and temperature; cluster radius; irrotational component $A_{g\theta}^0$, and solid body rotational component $B_{g\theta}^0$ of the gas and drop tangential velocities, respectively $u_{g\theta}^0 = A_{g\theta}^0 / r^0 + B_{g\theta}^0 r^0$ and $u_{d\theta}^0 = A_{d\theta}^0 / r^0 + B_{d\theta}^0 r^0$. u_{gr}^0 is calculated from the gas energy equation and $u_{dr}^0 = 0$.

The initial properties of gas (air) and liquid are also prescribed. For all calculations presented here $C_T = 0.05$ and $C_1 = 0.5$.

RESULTS

Previous results obtained with a 1110(1) cluster of uncharged droplets [1] showed that due to the larger gas temperature at the cluster inner and outer boundaries, the drop size decreases faster at those locations. Thus, if the Rayleigh limit is reached, it is first reached at either one of the cluster boundaries. In the present model the (110)Ds are followed up to the Rayleigh limit; further drop splitting which is beneficial because it provides secondary atomization is not modeled. If the Rayleigh limit is reached by drops at the inner boundary of the cluster, the computation is **Stopped** because the model does not describe the complex and unknown splitting process, and the drops located at larger radial coordinates would be affected by such important changes. If the Rayleigh limit is reached at the outer cluster boundary, the calculation is **pursued** and output of the drops having reached the Rayleigh limit are further ignored. This does not affect electrostatically the drops at smaller radial coordinates. It is assumed that because of the small drop size after drop splitting, the dynamic and thermodynamic effects on the gas are also small.

Since aromatic compounds play a major role in soot formation, all calculations presented here are performed for drops having benzene properties (Table 1). The results concentrate on the relative propensity to form soot precursors as indicated by the partial density of the evaporated compound, but independent of the chemistry. In order to understand the separate contributions of electrostatic dispersion which affects the drops radial motion, and that of gas and drop tangential irrotational motion and tangential solid body rotation, results were obtained for different initial conditions as shown in Table 2. In particular, it is desirable to know whether mechanical means can be used to accomplish the same degree of dispersion as the electrostatic charging, and whether mechanical dispersion can additionally be used to substantially enhance electrostatic dispersion.

The results discussed below are all from calculations performed with a binary drop size distribution ($R_1^0 = 2.0 \times 10^{-3}$ cm, $R_2^0 = 2.5 \times 10^{-3}$ cm) with $\Phi = 0.314$, $T_{g\infty}^0 = 600$ K, $T_{ds}^0 = 300$ K, $Y_{F\infty}^0 = 0.0$, $p = 1$ atm, $R_c^0 = 2$ cm, $u_{dr}^0 = 0.0$ cm/s, with $\max_{r_2}(n_2^0)/\max_{r_1}(n_1^0) = 1/3$. It is only the initial tangential velocities that are varied.

Direct (drop-induced), mechanical dispersion versus electrostatic dispersion

Drop charging results in a dramatic increase in the radial velocities and in a reduction of nonuniformities of the dependent variables as the cluster expands much faster, and the drop number densities for each initial-size class decrease; the consequence of these changes is to reduce the mass fraction of the evaporated compound and thus the propensity to form soot. The difference between drop-induced dispersion and electrostatic dispersion is best understood by examining plots of the velocity angle, θ , where $\tan \theta = |\vec{u}_{dr}| / |\vec{u}_{d\theta}|$ for both initial-size classes in runs 1 and 12. For uncharged drops, $\theta < 45^\circ$ and thus $|\vec{u}_{dr}| < |\vec{u}_{d\theta}|$. For charged drops, $\theta < 45^\circ$ in the inner part of the cluster and $\theta > 45^\circ$ in the outer part of the cluster; thus $|\vec{u}_{dr}| < |\vec{u}_{d\theta}|$ in the inner part of the cluster and $|\vec{u}_{dr}| > |\vec{u}_{d\theta}|$ in the outer part of the cluster. Therefore, dispersion is controlled by $\vec{u}_{d\theta}$ for Uncharged clusters, whereas dispersion is controlled by $\vec{u}_{d\theta}$ in the inner part of cluster and by \vec{u}_{dr} in the outer part of the cluster for charged clusters. Because $u_{d\theta} \simeq B_{d\theta}^0 r$ whereas $u_{d\theta} \simeq A_{d\theta}^0 / r$, runs 1-3 represent the most judicious way of mechanically enhancing dispersion in the outer portion of the cluster by increasing $\vec{u}_{d\theta}$.

Drop evaporation depends mainly upon T_{gi} , \vec{u}_{sj} and Y_{Fi} , all of which depend upon drop dispersion. As the drops disperse, the cluster engulfs hot, unvitiated air from the surroundings and this promotes evaporation. In cent rast, \vec{u}_{sj} decreases with increasing time, and this hinders evaporation. For uncharged clusters of drops, the relaxation of \vec{u}_{sj} continues throughout the drop lifetime, irrespective of the position within the cluster; for charged clusters of drops, a finite value of \vec{u}_{sj} is maintained in the outer portion of the cluster by the continuous contribution of the electrostatic force (which is an increasing function of r) to \vec{u}_{dr} . In this manner, electrostatic charging compounds the advantage of dispersion to evaporation.

• Effect of $A_{d\theta}^0$

Comparisons of results obtained in runs 3 and 4 show that for the very large irrotational motion chosen in these calculations, the drop number density increases substantially towards the inner cluster boundary and a front of drops is created which travels towards the outer boundary. In absence of charging, the drop number density is larger towards the inner cluster boundary and smaller toward the outer cluster boundary as the drop dispersion does not benefit of the added effect of the electrostatic charging. The result is a somewhat denser cluster, lower temperature (due to the larger amount of heat transferred to the drops) and larger Y_{Fi} (due to the compounded effect of the larger number of drops) towards the inner boundary, and the opposite towards the outer cluster boundary. Significantly, for uncharged drops, the larger ρ_{gi} at the locations of the lower temperature corresponds also to the location of the larger Y_{Fi} thus also increasing the value of $Y_{Fi}\rho_{gi}$; an increase in this value is an indication of more intense nucleation, producing a larger amount of soot precursors.

Since increases in $A_{d\theta}^0$ result in the formation of denser regions in the cluster thereby enhancing soot nucleation, no further calculations were performed with uncharged drops and larger values of $A_{d\theta}^0$ (trying to achieve mechanical dispersion equivalent to the charged drop dispersion) because it is obviously an unsuccessful approach.

• **Effect of $B_{d\theta}^0$**

Results from runs 1-3 were compared with those from run 12 to first determine the difference introduced by the electrostatic charge at otherwise identical conditions (runs 1 and 12), and second to explore the possibility of achieving dispersion similar to that induced by electrostatic forces by increasing the initial drop tangential solid body rotation (runs 2, 3 and 12).

Examination of the angle of the drop velocity vector with the tangential direction (Fig. 2) reveals that the maximum drop velocity angle for uncharged clusters or drops is near the cluster inner boundary and is almost insensitive to $B_{d\theta}^0$ (ranges from 33° to 35° for initial-size-class-1 and 37° to 42° for initial-size-class-2), whereas the maximum velocity angle for charged clusters of drops is near the outer boundary (68° for initial-size-class-1 and 57° for initial-size-class-2). This is because the maximum near the inner boundary is due to the acquired irrotational motion of the drops resulting from momentum transfer with the gas which is similar in runs 1-3, whereas the maximum near the outer boundary is due to the electrostatic force enlarging the radial component of the drop velocity. Additionally, the ranges of maximum velocity angles for the two initial-size classes show that when charging the drops according to $|q_d|_{\max} \sim R_d^0 [5]$, it is the smallest initial-size class that is preferentially dispersed, whereas in the absence of charge it is the largest initial-size class which is preferentially dispersed. Since smaller drops heat up faster, and thus evaporate faster, their preferential centrifugation promotes mixing and thus provides an additional benefit from electrostatic charging.

Increasing $B_{d\theta}^0$ results in increasing expansion, faster engulfment of hot gas by the cluster and thus faster evaporation. However, when the drops are uncharged, even for $B_{d\theta}^0 = 450 \text{ s}^{-1}$ and the same cluster expansion (Of 3.75 cm), the values of Y_{Fi} and ρ_{gi} are larger than when the drops are electrically charged and $B_{d\theta}^0 = 200 \text{ S}^{-1}$ [reached at $t = 2.52 \times 10^{-2} \text{ s}$ in the first case by which time the drops in initial-size-class-1 have all evaporated, and at $t = 1.6 \times 10^{-2} \text{ s}$ in the second case by which time the Rayleigh limit has been reached at the inner cluster boundary by drops from initial-size-class-1 whose maximum residual radius, $(R_1/R_1^0)_{\max}$, is 0.25]. It is not only the maximum values that differ in the uncharged versus the charged situation but also the profiles: the maximum Y_{Fi} occurs in the first case near the outer boundary and in the second case it appears as a plateau in the central part of the cluster. For uncharged drops, the maximum ρ_{gi} moves with increasing $B_{d\theta}^0$ from being near the outer boundary to being near the inner boundary; it is also near the inner cluster boundary in the charged drop case. The Y_{Fi} profile is determined by the drops motion and evaporation whereas the ρ_{gi} profile is determined by T_{gi} . Since nucleation of soot precursors depends upon $Y_{Fi}\rho_{gi}$, the fact that for low $B_{d\theta}^0$ the maxima of Y_{Fi} and ρ_{gi} occur at the same approximate location enhances the potential for soot nucleation.

Indirect (gas-induced) dispersion of charged drops

The above results show that direct mechanical dispersion cannot achieve the same reduction in $Y_{Fi}\rho_{gi}$ as electrostatic dispersion. It is though conceivable that mechanical dispersion added to electrostatic dispersion might contribute to a reduction in $Y_{Fi}\rho_{gi}$. Here we investigate gas-induced dispersion as different from direct, drop dispersion. The rationale is that it might be easier and more economic to produce gas-induced rather than drop-induced dispersion.

• **Effect of $A_{g\theta}^0$**

The value of $A_{g\theta}^0$ was decreased by a factor of 2 to 100 from run 6 to run 12 to investigate the influence of gas tangential irrotational motion upon charged drops. The larger gas irrotational motion is transferred to the drops and this induces a larger centrifugation at the inner cluster boundary creating a large moving front of drops at that location. Since the effect of the irrotational motion decreases as r^{-1} , the central and outer portion of the cluster do not benefit as much from the increased $A_{g\theta}^0$; in particular, initial-size-class-2 is more affected by the larger $A_{g\theta}^0$ since it is less centrifuged by the electrostatic force. The result of a larger $A_{g\theta}^0$ is an increase in the velocity angle at the inner boundary, and an increase in the nonuniformities of the chop number densities and residual radii. Comparisons between the Y_{Fi} and ρ_{gi} profiles for the two cases show that they are very similar except for somewhat lower values toward the inner cluster boundary.

Thus, within the range studied here, the gas tangential irrotational motion does not provide substantial additional centrifugation when the drops are charged. However, since by difference from the uncharged case, here it is the larger initial-size class which is most affected by $A_{g\theta}^0$, the gas irrotational motion might have the important role of enhancing the centrifugation of the larger, and thus more difficult to heat drops, and promoting their contact with the hotter surrounding gas.

• **Effect of $B_{g\theta}^0$**

The effect of the gas tangential solid body rotation has been studied by comparing results from several calculations: (1) runs 9-11 ($B_{g\theta}^0 = 100 \text{ s}^{-1}$, 200 S^{-1} , and 300 S^{-1} respectively) with $A_{g\theta}^0 = 100 \text{ cm}^2/\text{s}$ and $B_{d\theta}^0 = 200 \text{ s}^{-1}$, and (2) runs 6 and 8 ($B_{g\theta}^0 = 0 \text{ s}^{-1}$ and 100 s^{-1} , with $A_{g\theta}^0 = 200 \text{ cm}^2/\text{s}$ and $B_{d\theta}^0 = 200 \text{ s}^{-1}$).

The gas tangential solid body rotation is transmitted to the drops through momentum coupling and promotes the drops tangential motion. Since the solid body rotation becomes more important with increasing distance from the vortex center, it is only the outer part of the cluster that might be affected. Inspection of the results shows that the effect of $B_{g\theta}^0$ is negligible within the range studied. This is because on the one hand the larger drop tangential velocity results in a smaller velocity angle away from the inner cluster boundary thus tending to hinder dispersion, engulfment of hot

surrounding gas and evaporation; on the other hand, the larger drop tangential velocity at larger locations promotes drop heating and evaporation. The two effects balance for the range of $B_{d\theta}^0$ studied here and the values of Y_{Fi} and ρ_{gi} are very similar.

With increasing $B_{d\theta}^0$, it is expected that it is predominantly the smaller initial-size class which will be affected. If dispersion of these faster heating drops is hindered, this will somewhat counteract the beneficial electrostatic charge effect; if dispersion of these drops is enhanced, this will induce a spatial segregation by initial-size class whose effects on soot nucleation are difficult to assess a priori.

Direct (drop-induced) dispersion of charged drops

Drop-induced dispersion, although potentially more costly than gas-induced dispersion, might have a stronger effect when added to electrostatic dispersion because it dispenses with the otherwise necessary momentum transfer to achieve larger drop dispersion. Thus, we studied the effect of both initial drop tangential irrotational motion and solid body rotation.

• Effect of $A_{d\theta}^0$

As discussed above, a large $A_{d\theta}^0$ creates towards the inner cluster boundary a front of traveling drops, increases the drop number density and accordingly aggravates nucleation processes. Comparisons between results obtained with runs 5 and 12 show that for charged clusters of drops, the beneficial effect of charging is substantially decreased by increasing $A_{d\theta}^0$ from 0 to 200 cm²/s. At locations close to the inner cluster boundary, the large irrotational motion dominates the small electrostatic force and very large nonuniformities are created with larger n resulting in smaller T_{gi} , larger Y_{Fi} and larger ρ_{gi} than when $A_{d\theta}^0$ is null. At locations close to the outer cluster boundary, the irrotational motion is smaller and the electrostatic force dominates the drop's dispersion resulting in smaller departures from the situation when $A_{d\theta}^0 = 0$ cm²/s. The difference in dispersion between the two cases is best illustrated by the velocity angle: for null $A_{d\theta}^0$, the angle is <45° towards the inner cluster boundary whereas it is >50° towards the outer boundary and remains larger during the entire calculation for larger r ; for finite $A_{d\theta}^0$, the angle becomes >45° in the entire cluster and eventually decays to <45° towards the end of the calculation. When $A_{d\theta}^0 = 200$ cm²/s, parts of the cluster adjacent to the inner boundary remain in a dense configuration during the entire chop lifetime, thus defeating the purpose of the electrostatic charging.

• Effect of $B_{d\theta}^0$

Results from runs 7 and 12 were compared to investigate the effect of $B_{d\theta}^0$ on charged chops. Increasing $B_{d\theta}^0$ by 50% produced slightly increased cluster expansion. Due to the compounded effect of the larger solid body rotation and the electrostatic force, the velocity angle is (>45° and) smaller everywhere except at the inner cluster boundary (where it is similar) showing that as expected, \bar{u}'_{dr} is relatively smaller than $\bar{u}'_{d\theta}$. Both Y_{Fi} and ρ_{gi} have similar values in both calculations except at locations near the outer cluster boundary where they are slightly larger with increasing $B_{d\theta}^0$ due to the lower T_{gi} resulting from the larger n . The larger n is a direct consequence of the larger $B_{d\theta}^0$ at that location. Thus, it is interesting to notice that the benefits associated with electrostatic charging (in terms of potential soot nucleation) seem to decrease as $B_{d\theta}^0$ is increased.

SUMMARY AND CONCLUSIONS

The effect of mechanical dispersion on uncharged and electrostatically charged polydisperse clusters of drops has been numerically investigated. It has been shown that drop-induced mechanical dispersion cannot achieve the same beneficial effects as electrostatic dispersion in terms of decreasing both the mass fraction of the evaporated compound and the gas density to reduce soot nucleation while promoting evaporation. This is because increasing the drop tangential irrotational motion creates near the inner cluster boundary an increase in the drop number density that promotes soot formation. Increasing the chop tangential solid body rotation does disperse the cluster at locations further from its inner boundary; however, the slip velocity between chops and gas cannot be maintained, as it is for charged drops, and its added enhancement to evaporation is lost. Thus, electrostatic charging is superior to mechanical dispersion for soot control and enhancement of evaporation.

Since mechanical dispersion cannot compete with electrostatic dispersion, the idea of combining them to promote greater reduction in the partial mass fraction of the evaporated compound has been investigated as well. Both gas-induced and drop-induced dispersion were explored for charged clusters of drops. Within the range of values investigated, gas-induced tangential irrotational motion does not provide substantial additional dispersion for charged drops and thus does not contribute substantially to soot reduction. However, since the electrostatic charge is proportional to the initial drop radius and thus it disperses preferentially the smaller initial-size class, whereas the irrotational motion is most effective at smaller radial locations and thus affects the larger initial-size class which is less affected by the electrostatic force, the added effect of the gas tangential irrotational motion is to promote centrifugation of the larger drops through momentum transfer, and thus to enhance evaporation. A larger gas tangential solid body rotation has been seen to be ineffective for soot control within the range of values studied. This is because although the larger drop tangential velocity

results in a smaller velocity angle away from the inner cluster boundary thus tending to hinder dispersion, engulfment of hot surrounding gas and evaporation, it also promotes drop heating and evaporation. The two effects balance with no noticeable effect on the partial density of the evaporated compound. Drop-induced tangential irrotational motion has been shown to promote soot nucleation through the formation of a region of very large drop number density near the inner cluster boundary. Increasing the drops tangential solid body rotation did not affect central core near the inner boundary cluster regions, but increased the drop number density at the outer cluster boundary thereby promoting soot nucleation.

Thus, mechanical dispersion neither can compete with electrostatic dispersion to control soot nucleation, nor benefits noticeably soot control when added to electrostatic dispersion.

ACKNOWLEDGMENT

This research was conducted at the Jet Propulsion Laboratory and sponsored by the Office of Naval Research with Dr. Gabriel Roy serving as contract monitor, under an agreement with the National Aeronautics and Space Administration,

References

- [1] Law, C. K., Combustion Studies of Energetic Liquid Materials, Proceedings of the 7th ONR Propulsion Meeting, p.110, 1994
- [2] Sangiovanni, J. J. and Liscinsky, D. S., Soot Formation Characteristics of Well-Defined Spray Flames, *20th Symp. (Int.) on Combustion*, p. 1063, 1984
- [3] Bellan, J. and Harstad, K., Electrostatic Dispersion and Evaporation of Clusters of Drops of High-Energy Fuel for Soot Control, *26th Symp. (Int.) on Combustion*, p. 1713-1722, 1996
- [4] Santoro, R. J., private communication, 12/1/1995
- [5] Kelly, A. J., The Electrostatic Atomization of Hydrocarbons, *J. of Inst. of Energy*, vol. 51.110.431, p. 312-320, 19 S-1
- [6] Bellan, J. and Cuffel, R., A Theory of Non Dilute Spray Evaporation Based upon Multiple Drop Interactions, *Combust. and Flame*, vol. 51, p. 55-67, 1983
- [7] Harstad, K. and Bellan, J., Behavior of a Polydisperse Cluster of Interacting Drops Evaporating in an Inviscid Vortex, accepted for publication in the *Int. J of Multiphase Flow*
- [8] Hidy, G. M. and Brock, J. R., The Dynamics of Aerocolloidal Systems, *International Reviews in Aerosol Physics and Chemistry*, Vol 1, Pergamon Press, 1970

NC) MENCLATURE

A	irrotational part of the velocity	Greek symbols	
B	solid body rotation part of the velocity	θ	angular coordinate
C_1	constant in the Nusselt number expression	μ	viscosity
C_T	proportionality constant for μ_T	ρ	density
n	drop number density	Φ	air/fuel massratio
Nu_c	cluster Nusselt number	Subscripts	
p	pressure	c	cluster
Pr	Prandtl number	d	drop
$ q_d _{\max}$	maximum drop charge (see [5])	ds	drop surface
r	radial coordinate	F	fuel
R_c	outer cluster boundary	g	gas
R_{in}	inner cluster radius	i	interstitial
R_j	radius of initial-size-class j	j	initial-size-class
Re	Reynolds number	s	slip
Sc	Schmidt number	T	turbulent
t	time	θ	tangential direction
T	temperature	∞	far field
u	velocity	Superscripts	
	mass fraction	0	initial

Property	Value
stoichiometric air/fuel mass ratio	13.2
molecular weight, g/mole	78.12
normal boiling point, K	353
latent heat at normal boiling temperature, cal/g	96.90
$\Delta C_p = C_{pl} - C_{pg}$, cal/(gK)	6.8×10^{-2}
liquid density, g/cm³	0.879
liquid heat capacity at constant p: C_{pl}, cal/(gK)	0.415
liquid viscosity, g/(cms)	0.392×10^{-2}
liquid mass diffusion coefficient for a Lewis number of 10, cm²/s	0.995×10^{-4}
liquid thermal conductivity, cal/(gK)	3.63×10^{-3}
gas heat capacity at constant p: $C_{pg}(T_g = \sqrt{300 \times 600})$, cal/(gK)	0.37

Table 1: Properties of benzene

Run #	% of $ q_d _{\max}$	$A_{d\theta}^0$, cm ² /s	$B_{d\theta}^0$, s ⁻¹	$A_{g\theta}^0$, cm ² /s	$B_{g\theta}^0$, s ⁻¹
1	0	0	200	100	0
2	0	0	350	100	0
3	0	0	450	100	0
4	0	200	200	100	0
5	0.25	200	200	100	0
6	0.25	0	200	200	0
7	0.25	0	300	100	0
8	0.25	0	200	200	100
9	0.25	0	200	100	100
10	0.25	0	200	100	200
11	0.25	0	200	100	300
12	0.25	0	200	100	0

Table 2: Percent of maximum charge and initial conditions for, velocities.

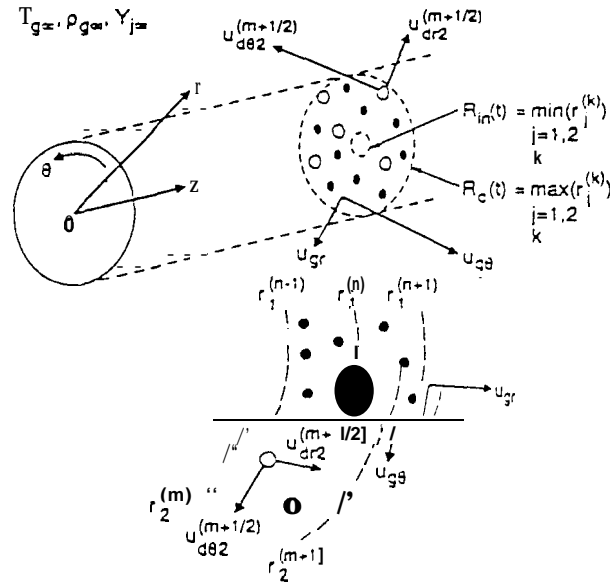
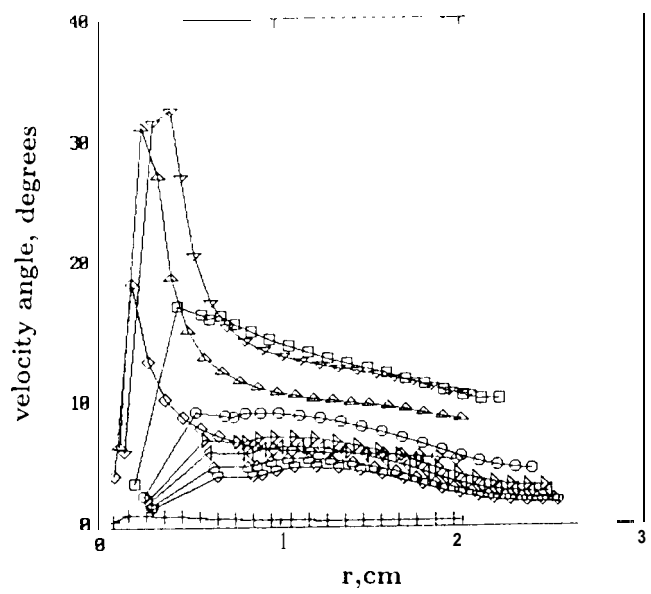
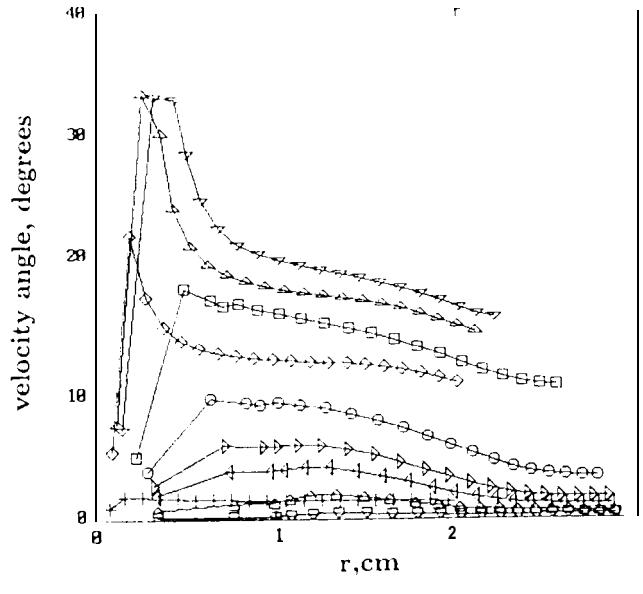


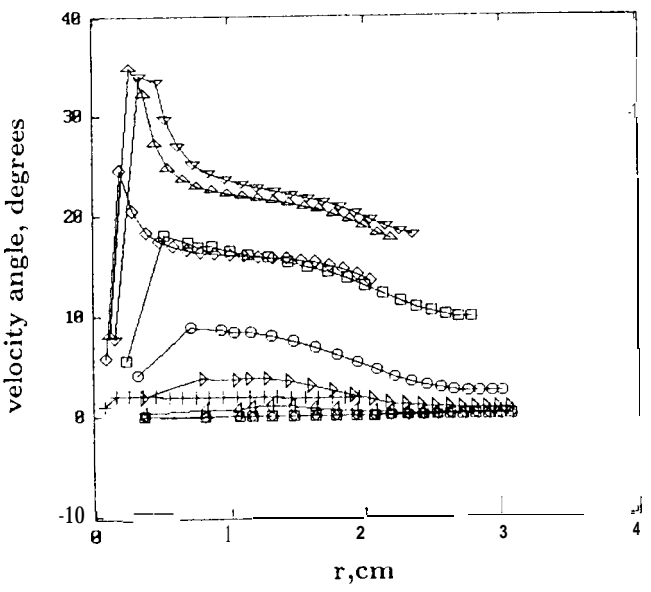
Figure 1. Physical configuration of the cluster-in-vortex for a binary size distribution.



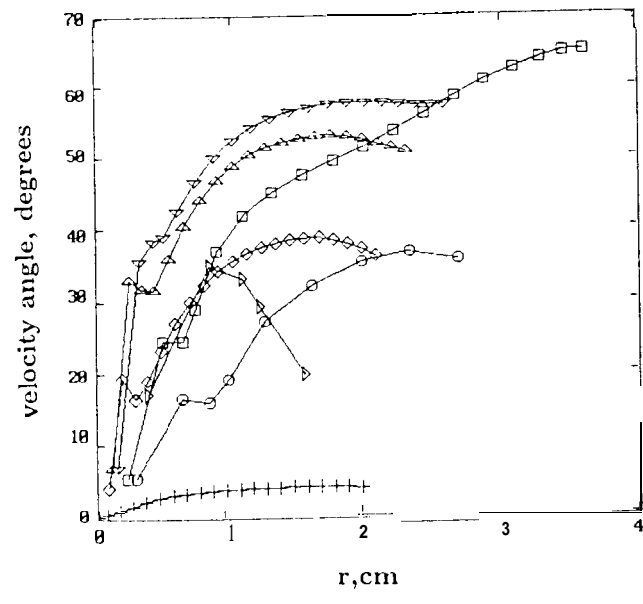
a



b



c



d

Figure 2. Velocity angle for initial-size-class-1 for runs 1 (a); 2 (b); 3 (c); and 12 (d). Symbols correspond to times as follows: $8.37 \times 10^{-5}s$ (+); $9.29 \times 10^{-5}s$ (\diamond); $1.76 \times 10^{-3}s$ (\triangle); $2.60 \times 10^{-3}s$ (∇); $5.94 \times 10^{-3}s$ (\square); $1.18 \times 10^{-2}s$ (\circ); $1.60 \times 10^{-2}s$ (\triangleright); $1.85 \times 10^{-2}s$ (\triangleleft); $2.19 \times 10^{-2}s$ ($\hat{\square}$); and $2.52 \times 10^{-2}s$ (\square).